ACS NANO

www.acsnano.org

ARTICLE

An Ingestible Self-Polymerizing System for Targeted Sampling of Gut Microbiota and Biomarkers

Lu Chen, Lina Gruzinskyte, Steffen Lynge Jørgensen, Anja Boisen, and Sarvesh Kumar Srivastava*

Cite This: *ACS Nano* 2020, 14, 12072–12081

Read Online

ACCESS | Metrics & More | Article Recommendations | Supporting Information

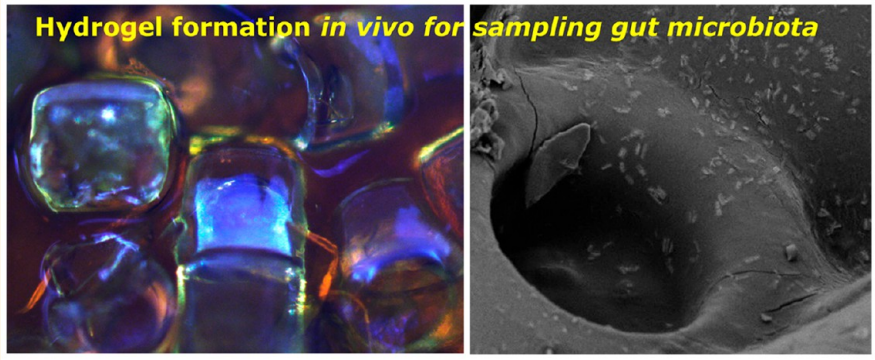

ABSTRACT: A proof-of-concept for the fabrication of a self-polymerizing system for sampling of gut microbiome in the upper gastrointestinal (GI) tract is presented. An orally ingestible microdevice is loaded with the self-polymerizing reaction mixture to entrap gut microbiota and biomarkers. This polymerization reaction is activated in the aqueous environment, like fluids in the intestinal lumen, and causes site-specific microsampling in the gastrointestinal tract. The sampled microbiota and protein biomarkers can be isolated and analyzed *via* high-throughput multiomic analyses. The study utilizes a hollow microdevice (Su-8, *ca.* 250 μm), loaded with an on-board reaction mixture (iron chloride, ascorbic acid, and poly(ethylene glycol) diacrylate monomers) for diacrylate polymerization in the gut of an animal model. An enteric-coated rat capsule was used to orally gavage these microdevices in a rat model, thereby, protecting the microdevices in the stomach (pH 2), but releasing them in the intestine (pH 6.6). Upon capsule disintegration, the microdevices were released in the presence of luminal fluids (in the small intestine region), where iron chloride reacts with ascorbic acid, to initiate poly(ethylene glycol) diacrylate polymerization *via* a free radical mechanism. Upon retrieval of the microdevices, gut microbiota was found to be entrapped in the polymerized hydrogel matrix, and genomic content was analyzed *via* 16s rRNA amplicon sequencing. Herein, the results show that the bacterial composition recovered from the microdevices closely resemble the bacterial composition of the gut microenvironment to which the microdevice is exposed. Further, histological assessment showed no signs of local tissue inflammation or toxicity. This study lays a strong foundation for the development of untethered, non-invasive microsampling technologies in the gut and advances our understanding of host–gut microbiome interactions, leading to a better understanding of their commensal behavior and associated GI disease progression in the near future.

KEYWORDS: *gastrointestinal tract, radical polymerization, gut microbiota, 16s rRNA amplicon sequencing, protein biomarkers*

Despite tremendous progress made by next-generation sequencing, the very first step in a microbiome study is the collection of microbial biomass samples, which poses a significant challenge. While a stool sample has high microbial density,[1] microbiome analysis *via* stool sampling is inadequate because of: (1) an inability to capture all the

Received: June 30, 2020
Accepted: August 19, 2020
Published: August 24, 2020

https://dx.doi.org/10.1021/acsnano.0c05426
ACS Nano 2020, 14, 12072–12081

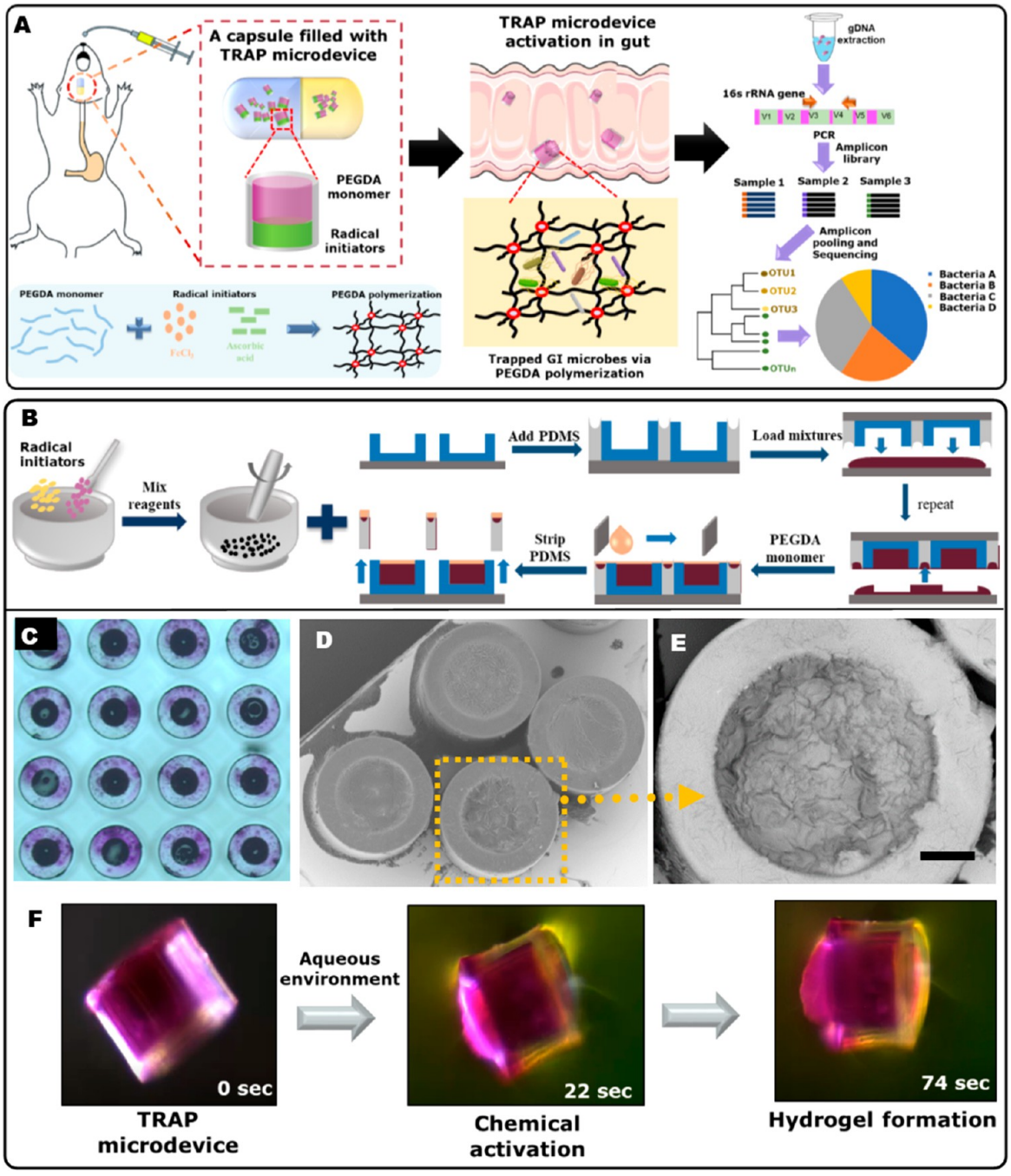

Figure 1. (A) Schematic representation of TRAP microdevice for gut microsampling: oral administration in a capsule with inset highlighting the reaction components, activation of hydrogel *in vivo* for entrapping gut microbiota and 16s RRNA amplicon sequencing from isolated TRAP microdevices. (B) Schematic representation of TRAP microdevice fabrication. (C) Optical image of a loaded TRAP microdevices upon peeling of PDMS mask. (D) SEM microgrph of fabricated TRAP microdevices. (E) SEM micrograph (BE) of a TRAP microdevice showing rough surface topography. Scale bar 50 μm . (F) TRAP microdevice activation over a period of time.

microorganisms in the upper gastrointestinal (GI) tract and (2) an inability to maintain spatial distribution of different microbes in the GI tract.[2,3] Other techniques, including mucosal brushing[4] and rectal swabs,[5] lack protocol consistency, while colonoscopy/endoscopy (biopsy) have a low patient compliance.[6] To this end, self-activated micromotors technology has shown great potential with studies like collapsible microgrippers for cell capturing (*in vitro*)[7,8] and self-propelling microdevices for delivery of therapeutics (*in vivo*).[9,10] Simply speaking, these microdevices trigger a chemical reaction under specific environments (*e.g.*, heat, pH, body fluids), which in turn causes them to propel or to undergo physical deformation (*i.e.*, chemical actuation).[11] An untethered GI sampling technique, to capture gut microbiome and protein biomarkers, is of tremendous interest for gut engineering.[12]

DISCUSSION

This work demonstrates oral administration of an ingestible microdevice that can self-polymerize in the gut of a murine model to enmesh site-specific microbiota and biomarkers.

https://dx.doi.org/10.1021/acsnano.0c05426
ACS Nano 2020, 14, 12072−12081

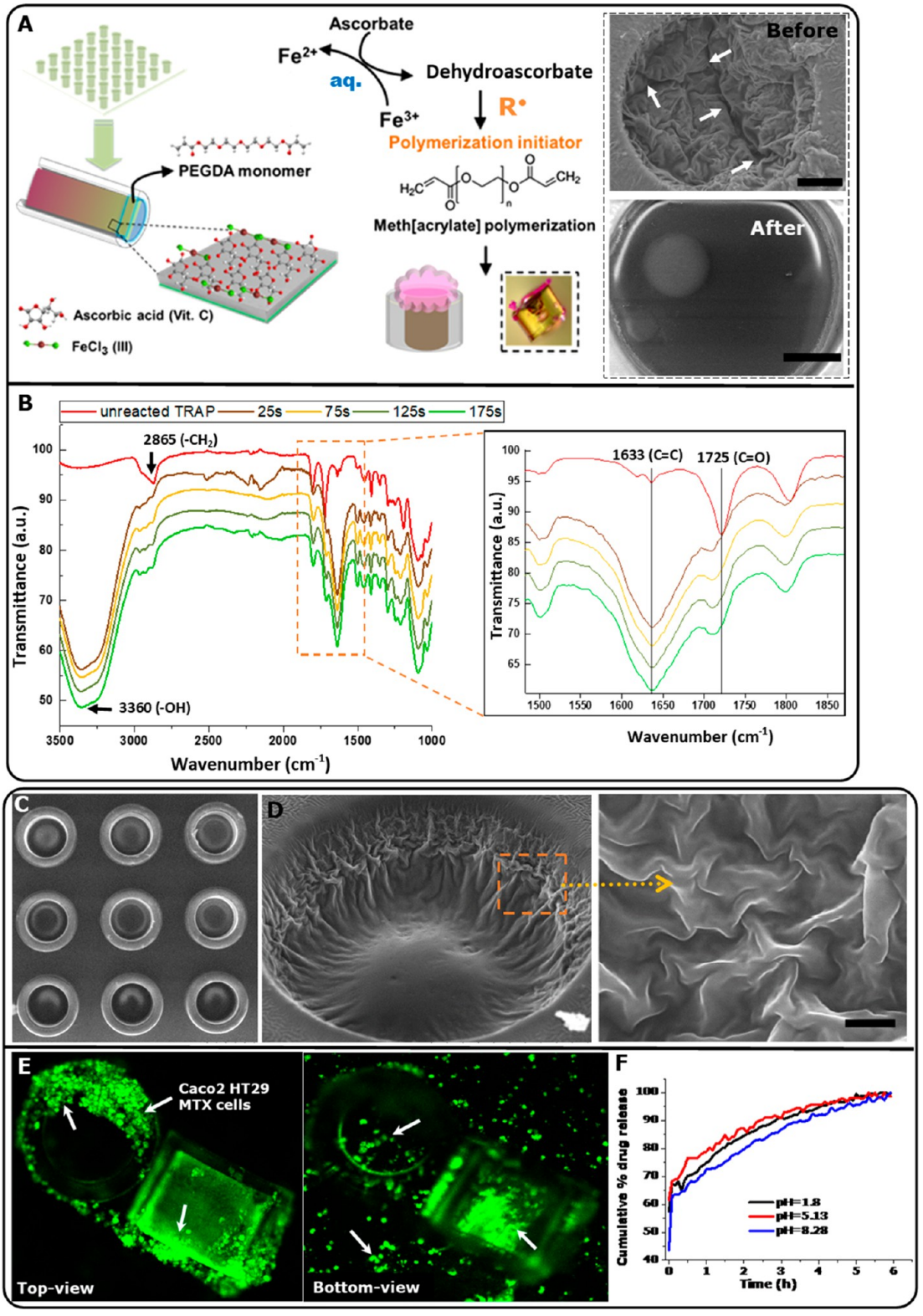

Figure 2. TRAP microdevice. (A) Reaction mechanism (inset shows the top view of the microdevice "before" and "after" PEGDA polymerization; Scale bar: 50 μm). "White arrows" depict surface cracks and crevices. (B) ATR-FTIR spectra of real-time hydrogel formation. (C) SEM micrograph of multiple activated TRAP microdevices with distinct hydrogel formation inside the microdevice. (D) SEM micrograph showing inside of an activated TRAP microdevice (hydrogel). Inset shows a distinct "highly wrinkled" surface morphology. Scale bar: 2 μm. (E) Confocal fluorescence imaging of Caco-2/HT29-MTX cells trapped inside the hydrogel. Fluorescence FITC-insulin (Ex/Em: 495/525 nm). (F) TRAP microdevices for potential drug release kinetics (R6G as a model drug) at varying pH simulating the GI tract: stomach (pH 2), intestine (pH 5.2), and colon (pH 8).

https://dx.doi.org/10.1021/acsnano.0c05426
ACS Nano 2020, 14, 12072−12081

Fabricated with a biocompatible photopolymer SU-8, these microdevices resemble a hollow cylindrical geometry, which is loaded with PEGDA monomers, $FeCl_3$ (III), and ascorbic acid (vitamin C), as shown in Figure 1A. Based upon a targeted radical polymerization in the gut, these TRAP microdevices (*ca.* 250 μm) were loaded inside an enteric-coated gelatin capsule for oral administration. The enteric coating prevents capsule disintegration in the stomach (pH 2), but degrades in the intestine (pH 6−7) to release TRAP microdevices. Once released, TRAP microdevices react with the luminal fluids (in the intestine) and form a polymeric PEGDA hydrogel, thereby, effectively trapping gut microbiota and protein biomarkers. Finally, enmeshed microbiota can be analyzed *via* a high-throughput sequencing (HTS) method, like 16s rRNA amplicon sequencing, as demonstrated in our study.

The detailed fabrication process of TRAP microdevices is displayed in Figure 1B. Before loading, a Si substrate incorporating microdevice structures was coated with a thin layer of PDMS, which acted as a negative mask as reported by Kamguyan *et al.* A radical-initiator mixture comprising of ascorbic acid and iron(III) chloride was loaded inside the hollow device cavity and was sealed with a layer of PEGDA monomer. Finally, the thin layer of PDMS was peeled-off, and individual TRAP devices were obtained (Figure 1C). Successful loading of TRAP microdevices was also confirmed *via* scanning electron microscopy (SEM), as shown in Figure 1D. Interestingly, a backscattered SEM micrograph (Figure 1E) confirmed that the PEGDA monolayer on top is not smooth but rough. This rough topography supports PEGDA polymerization when in contact with aqueous fluids. Reactant mixture can also be loaded by mixing together, though a hydrophobic PDMS layer (as in our case), and may lead to uneven loading of microdevices. Upon exposure to aqueous environment, radical polymerization gets triggered causing PEGDA polymerization, as shown in Figure 1F.

Figure 2A describes a PEGDA hydrogel formation mechanism inside a TRAP microdevice. When a TRAP microdevice is exposed to an aqueous environment, iron(III) chloride/ascorbic acid acts as a redox initiator for free-radical generation.[13,14] In the presence of oxygen, ascorbic acid is oxidized to dehydroascorbic acid, which involves a two-electron transfer.[15] Ascorbate radicals have been previously employed for initiation of acrylonitrile polymerization. The reaction scheme can be postulated as follows (AH_2: ascorbic acid; AH: ascorbate radical; A: dehydroascorbic acid):

$$AH_2 \xrightarrow[\text{slow}]{} A^{\bullet}H + HO_2^{\bullet} + HO_2^{\bullet} \xrightarrow[\text{very fast}]{} A + H_2O_2$$

$$AH_2 + A \xrightarrow[\text{very fast}]{} 2A^{\bullet}H$$

Further, it has been demonstrated that a Fenton-like reaction proceeds to a Fe(III)/H_2O_2 system, where spontaneous reaction of H_2O_2 with Fe(III) primarily forms iron(III)-hydroperoxo complexes.[16,17] Once formed, the iron(III)-hydroperoxo complexes are assumed to decompose in a unimolecular way to regenerate Fe(II) and to yield $HO_2^{\bullet}/O_2^{\bullet-}$ and $OH^{\bullet}$ radicals as follows:[18,19]

$$Fe^{3+} + H_2O_2 \underset{K_1}{\Leftrightarrow} FeOOH^{2+} + H^+$$

$$Fe^{2+} + H_2O_2 \rightarrow Fe^{3+} + HO^- + HO^{\bullet}$$

$$O_2^{\bullet-} + Fe^{3+} \rightarrow O_2 + Fe^{2+}$$

Kinetic studies have confirmed that the rate of decomposition of H_2O_2 by Fe(III) depends on pH, initial concentrations of Fe^{III} and H_2O_2, ratios of H_2O_2 to Fe^{III} concentrations, and complexation of Fe^{III} by organic and inorganic ligands.[17,20] In fact, ionic iron complexes and bulky onium cations with halide anions (like chloride, bromide, or iodide) have been used for polymerization of acrylates by both direct and reverse atom-transfer radical polymerization.[21] This reaction cascade triggers a chain-growth polymerization by propagation of active centers through acrylate-end groups containing multiple —C═C— bonds activating *in situ* PEGDA hydrogel formation. Here, it should be noted that rate of radical polymerization strongly depends on the rate of free radical generation, which in turn depends upon the choice of radical initiator.[22]

Figure 2A (inset) shows a SEM micrograph depicting a rough PEGDA monomeric layer (labeled as "before"), with cracks and crevices of *ca.* 5−10 μm (marked by "white arrows"). These microcracks facilitate the entry of aqueous solution inside the microdevice and acts as "reaction microcenters" to initiate PEGDA polymerization. Also, heating at mild temperature and storage in a vacuum desiccator remove excess moisture, if any, and pack the reaction mixture together inside the microdevice. Since PEGDA monomer (Mn: 575 g/mol) is highly viscous as compared to water, that is, 57 cP *vs* 1 cP, once loaded inside a microdevice, the TRAP microdevice is greatly dominated by viscous forces ($Re < 1$). Therefore, partial loss of PEGDA monomer is minimal, and owing to the microconfinement effect inside the device, polymerization tends to proceed along the inner cavity of the microdevice[23] (see Supporting Information Figure S1).

Upon completion of polymerization, a distinct hydrogel formation is visually identifiable (Figure 2A, inset: "after"). PEGDA hydrogel formation inside a TRAP microdevice was investigated *via* an ATR-FTIR spectroscopy (Figure 2B). Unreacted TRAP (red line) has a distinct peak at 2865 cm^{-1} corresponding to an unreacted (CH_2) terminal group which disappears as the reaction proceeds (upon incorporation of water to trigger the reaction). The intensity of the stretching vibration at 1630 cm^{-1} (vC═C) overlapped with OH angular deformation from water, which could explain the existence of this band in the polymerized PEGDA spectrum (Figure 2B inset). The band at 1635 cm^{-1} can be attributed to a reaction product of OH^- and oxidized products of ascorbate produced during the Fe^{3+} reduction.[24,25] A similar observation was also made by Lee *et al.* for reducing PEGDA hydrogel formation in the presence of citric acid and Au^{3+} reduction.[26] Polymer chain extension was further confirmed with the shifting of a carbonyl band (1730 cm^{-1}) of the acrylate group (Figure 2B inset). Finally, characteristic hydrogel swelling (OH peak) was confirmed at 3360 cm^{-1} region, growing gradually over a period of time (*ca.* 3 min), which was absent prior to the reaction. Figure 2C shows a SEM image of multiple TRAP microdevices showing distinct hydrogel formation; also see Supporting Information Video S1 showing real-time hydrogel formation in multiple TRAP microdevices. Interestingly, hydrogel swelling resulted in a characteristic polymer swelling (Figure 2D) with a distinct mesh-like morphology (as demonstrated in the inset image). For efficient GI micro-sampling, TRAP microdevices must operate in the presence of a thick mucus layer (30−450 μm),[27,28] while they secure the site-specific microbiota and biomarkers. This is an important

https://dx.doi.org/10.1021/acsnano.0c05426
ACS Nano 2020, 14, 12072−12081

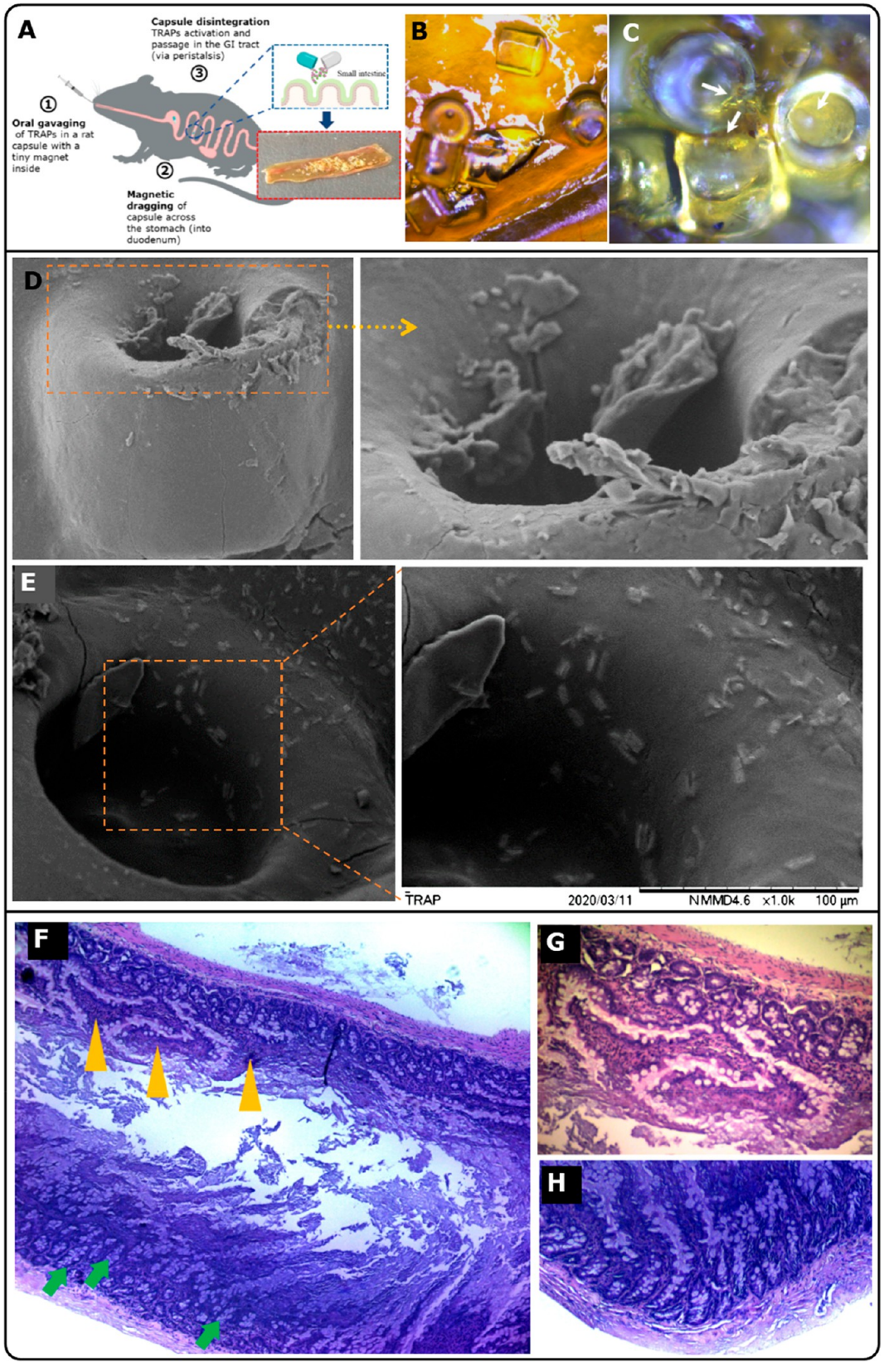

Figure 3. Oral administration of TRAP microdevices (in a rat model). (A) Schematic representation of oral gavaging experiment. Inset shows uniform distribution in the upper ileum region of the GI tract. (B) Optical microscopy images of TRAP microdevices over the excised intestine tissue. (C) Hydrogel formation in the gut of a rat model. (D) SEM micrograph of an activated TRAP microdevice in a rat's ileum. Inset shows PEGDA hydrogel fibrils covering the microdevice. (E) SEM micrograph depicting enmeshed gut bacteria. Inset image shows distinct rod-shaped bacteria trapped over the microdevice surface. (F) Histology of the excised intestine tissues processed with H&E staining; Crypts: "green arrow" and villi: "yellow arrow". (G) Uniform crypts (mag: 20×) and (H) normal villi.

https://dx.doi.org/10.1021/acsnano.0c05426
ACS Nano 2020, 14, 12072−12081

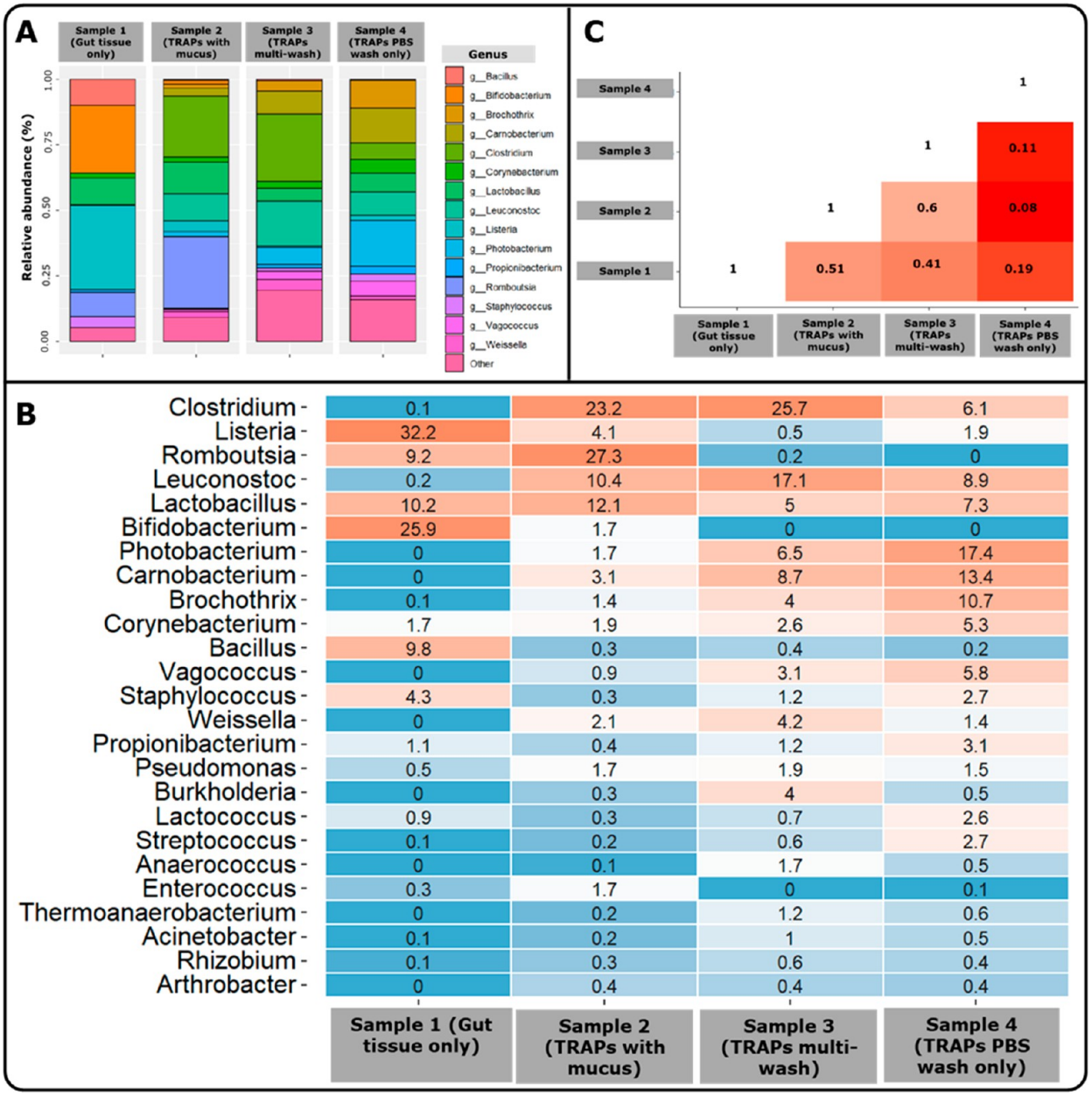

Figure 4. Effect of washing on recovered TRAP microdevices for gut microbiota assessment. (A) Stacked bar plot of top 15 most abundant genera. (B) Heatmaps of the 25 most abundant genera. (C) Bray–Curtis dissimilarities–distance plot between the three samples.

consideration since the bulk viscosity of mucus secretions, which is approximately 2000-fold more viscous than water at low shear, poses a significant challenge for any physical deformation *via* a chemically activated microdevice.[29]

Therefore, we opted for a co-culture of Caco-2 and mucus producing HT29-MTX-E12 human colon cancer cells to demonstrate cell trapping in the presence of mucus and to highlight potential for therapeutics delivery. TRAP microdevices were loaded with fluorescein isothiocyanate (FITC)-insulin and incubated in a co-culture petridish for 4 h, washed with PBS buffer, and observed under a confocal microscope. Figure 2E shows cellular uptake of FITC-insulin delivered *via* TRAP microdevices. In fact, fluorecent cells were found to be enmeshed in the hydrogel matrix, both inside and outside the device (marked with "white arrows"). Incorporation of a fluorescently tagged biologic (FITC-insulin) provided three key-benefits: (1) easy identification of cells trapped in an otherwise transparent hydrogel matrix;[8] (2) successful diffusion of therapeutics in the presence of GI mucus (dynamic viscosity: 80 cP *vs* 1 cP of water);[30,31] and (3) potential to carry small molecule therapeutics and biologics with a distinct pH-dependent release profile (Figure 2F). We also demonstrated trapping of *Escherichia coli* bacteria stained with Bactlight Red dye (see Supporting Information Figure S2).

Finally, TRAP microdevices were loaded in a gelatin capsule, together with a tiny magnet, and orally gavaged in a rat model (Figure 3A). The role of tiny magnet was to ensure that the gelatin capsule does not disintegrate in the stomach and was magnetically dragged into the duodenum. Once in the small intestine (~pH 6.8) region, the enteric-coated (Eudragit L-100) capsule was disintegrated, and TRAP microdevices were released. After oral administration (3 h), TRAP microdevices were localized *ca.* 25 cm downstream from the stomach, in the ileum region. It must be noted that the magnet has no role in

https://dx.doi.org/10.1021/acsnano.0c05426
ACS Nano 2020, 14, 12072–12081

activation or subsequent localization of TRAP microdevices in the ileum region, which is governed by the natural motion of the GI tract (*i.e.*, peristalsis). Figure 3B depicts TRAP microdevices over the excised intestinal tissue. Upon exposure to the luminal fluids, TRAP microdevices were successfully "triggered" inside the GI tract of the rat model (Figure 3C). This was further confirmed by SEM micrographs of the excised tissue with TRAP microdevices (with a thin layer of Au). Figure 3D depicts hydrogel formation *in vivo* with polymerized PEGDA structures extruding out from the microdevice. Incidentally, we were able to observe surface-enmeshed bacteria (rod-shaped) over a TRAP microdevice, as shown in Figure 3E. Also, refer to Supporting Information Figure S3 showing optical microscopy images and SEM micrographs of TRAP microdevices after the animal experiment.

We also evaluated the toxicity of TRAP microdevices *via* histological assessment of the excised gut tissue. Essentially, reaction mixture of TRAP technology is highly biocompatible, comprising of iron chloride (III) and vitamin C. Further, incorporation of low molecular weight PEGDA monomers showed no visible signs of toxicity as confirmed by hematoxylin and eosin (H&E) staining. Figure 3F shows a cross-sectional area of the excised small intestine tissue with unaffected mucosa characterized by slender villi (Figure 3G) and uniform crypts (Figure 3H), showing no signs of cellular inflammatory response. This is also understandable since acute oral LD_{50} toxicity of acrylate monomers in the rat model is 10−20 g/kg, while the total administered dosage in the experiment was <1 mg (density: 1.12 g/mL), *ca.* 10,000 times less than the minimum dosage.[32,33] Likewise, the ingenuity of a slow redox polymerization mechanism, packed inside an enclosed microchamber, minimizes exposure of free radicals to the outside tissue, thereby, minimizing toxicity.

Finally, excised TRAP microdevices were isolated and analyzed for gut microbiota assessment (Figure 4); also refer to Supporting Information Figure S4 depicting protein (trypsin) biomarker assessment. Herein, the main idea was to verify that the gut microbiota can be enmeshed in the gel matrix inside the microdevice and that the genomic content can be isolated for subsequent HTS analyses. Four sample groups included: (1) excised gut tissue only (GI tissue region from where the ingested TRAP microdevices were recovered); (2) scrapped mucus (with TRAPs); (3) TRAPs thoroughly washed with acetate buffer (pH 4), PBS, and 70% EtOH a total of nine times, to clean the microdevice surface of excess mucus and other surface-contaminants; and (4) TRAPs washed with PBS only. After the washing protocol, microdevices were harvested *via* a ball-milling process, and recovery of microbial DNA was carried out (see Supporting Information Table S1 for secondary index PCR data).

Table 1 describes different alpha diversity indexes at the genus level for each sample. The samples were rarefied at 294,135 reads to compare the alpha diversity. See Supporting Information Figure S5 for rare faction curves. We observed the lowest number of operational taxonomic units (OTUs) in sample 1, followed by samples 2, 3, and 4, respectively. This was also represented in the Shannon diversity index indicating that sample 1 has a lower species richness and a more uniform composition as compared to samples 2, 3, and 4, indicating that few genera dominates sample 1. This is understandable since sample 1 is comprised of excised "gut tissue only", which is rather homogeneous in its microbial makeup.

Table 1. Different Alpha Diversity Indexes at Genus Level for Each Sample

sample name	total reads	raw reads	observed OTUs	Shannon
sample 1 (gut tissue only)	102,881	45,054	45	1.982535
sample 2 (TRAPs w/ scrapped mucus)	257,868	223,787	91	2.391751
sample 3 (TRAPs multiwash)	308,493	294,135	106	2.792572
sample 4 (TRAPs PBS wash only)	232,789	220,747	123	2.889607

Figure 4A depicts the relative abundance of bacterial genera between the four samples using 16s rRNA amplicon sequencing. The stacked bar plot demonstrated that few genera are very abundant in sample 1 (*i.e.*, gut tissue only), which was highlighted in the alpha diversity analysis too. More detailed information is presented in Figure 4B showing the heatmap of the 25 most abundant genera in the samples. Sample 1 was dominated by six genera: *Listeria*, *Bifidobacterium*, *Lactobacillus*, *Bacillus*, *Romboutsia*, and *Staphylococcus spp.* (also see Supporting Information S6). All of these microbes are also the original residents of a rat's GI tract.[34] *Lactobacillus* and *Bifidobacterium sp.* are lactic acid and carbohydrate-fermenting bacteria responsible for short-chain fatty acid production in a murine model.[35,36] Interestingly, *Romboutsia spp.* is a natural and abundant inhabitant of the rat small intestine[37] and is a nonmotile obligate anaerobe, which generally resides under the thick mucus layer.[38] Therefore, isolation and detection of the *Romboutsia sp.* in sample 2 is a potential sampling technique for microbiota detection in the intestinal crypt buried deep within the mucus.

Relative variation in microbial population was expected and also observed in our study due to three main reasons: (1) varying "zone of activation" for each individual microdevice; (2) heterogeneity of GI microbiota and mucus layer thickness within the same GI region; and (3) disintegration of ingested capsule upstream of the ileum region (from where the microdevices were recovered). This could also explain low levels of *Clostridium sp.* and *Leuconostoc sp.* in Sample 1 as compared to the other samples, where the TRAP microdevices moved along the natural flux in the GI tract (peristalsis). An exhaustive study by Li *et al.* also reported both intersubject variations from the phylum to genus levels (in Sprague−Dawley rats) and higher intersubject variations in samples from the upper GI tract than from the lower GI tract.[34] Another reason for variation between different groups could be attributed to the cross-section of the gut tissue sample being analyzed (which is a small section as compared to the entire length of the tissue bearing microdevices). This variation was also supported with A Bray−Curtis distance−dissimilarity distance plot between the four samples (Figure 4C). As expected, samples 2 and 3 were slightly more similar to sample 1 (0.51 and 0.41 respectively) than sample 4 (0.19). This indicates that our multistep washing protocol could potentially remove certain surface-bound bacteria as observed with *Listeria sp.* and *Romboutsia sp.* These differences could be both due to the biological or technical variations (as discussed above) and will be a part of our future investigations. Another important area of research will be to optimize the microdevice design, minimize cross contamination, and facilitate non-invasive sampling of the GI tract.

https://dx.doi.org/10.1021/acsnano.0c05426
ACS Nano 2020, 14, 12072−12081

CONCLUSION

This study lays a strong foundation toward orally ingestible microdevices for microbiome sampling in the upper GI tract *via* an *in situ* polymerization method. We demonstrated that a targeted radical polymerization (TRAP) technology can enmesh cells, bacteria, and enzyme biomarkers from the upper GI tract of an animal, in a relatively nontoxic manner.

One of the key unmet needs in the area of gut microbiome research is to determine the relative importance of luminal and mucosal-associated microbiota in normal homeostatic and disease-inducing and/or disease-perpetuating activities.[39] To this end, we demonstrated that TRAP microdevices can sample both luminal and mucus-binding microbiota (like *Romboutsia sp.*), for subsequent high-throughput analyses. Likewise, TRAP microdevices can also be used to isolate obligate anaerobes, which account for over 50% of the gut microbiome, for subsequent subculturing and analyses. This will play a key-role in fecal microbiota transplantation where it remains a challenge to understand ecological forces that shape the microbiota. The next generation of such ingestible self-polymerizing microdevices will facilitate non-invasive biopsy and untethered microsampling of a wide range of cells, pathogens, and biomolecules in the GI tract. This will also provide an improved understanding of GI disease progression (like inflammatory bowel disease, ulcerative colitis, and Crohn's disease, among others), which are heavily modulated by the host microbiota (together with existing animal models).

Gut microbiome is complex, as there are high levels of variation even within the same GI site of an animal, which depends on mucus thickness, food intake, and complex commensal behavior, among others. The future of TRAP technology will address issues pertaining to sampling bias (relative *vs* absolute abundance) and device toxicity (with minimal chances of accidental retention). A multidisciplinary effort in the area of polymer engineering, microfabrication, and multiomics will push the frontiers of *precision* gut microsampling, which is poised to have a significant impact on both fundamental sciences and applied healthcare. Precise identification of bacterial communities will allow a greater understanding of host−microbiome interactions, paving a way for personalized gut therapies in the future.

EXPERIMENTAL SECTION

Fabrication of TRAP Microdevices. The conventional epoxy-based negative photoresist SU-8 (MicroChem, USA) was used to fabricate the microcontainers (hollow cylindrical structures) using a two-step photolithography technique. The first layer of SU-8 (2035, 69.95 wt %) was spin coated (Süss MicroTec RCD8 with Gyrset) on a fluorocarbon-coated silicon wafer and soft baked at 50 °C for 2 h (temperature ramping at a rate of 2 °C/min) and slowly cooled down to room temperature. The bottom of the microcontainers (thickness 35 μm) was defined using UV exposure for 30 s using soft contact (Süss Mask Aligner MA6, equipped with in-line notch filter) as well as two bursts of 250 mJ/cm^2. A post-exposure baking was conducted at 50 °C for 6 h (with the same ramping conditions as mentioned before). The second layer of resist (SU-8 2075, 73.45 wt %) was spin coated and prebaked at 50 °C for 10 h to define the microwell wall (height 220 μm) using the same temperature ramping condition. A global WEC chuck was used to conduct the UV exposure in proximity mode, followed by two bursts of 250 mJ/cm^2 for 30 s, after which a post-exposure baking was performed at 50 °C for another 10 h using the same temperature ramping condition. The resulting substrate was developed in mr-Dev 600 for 2 × 20 min. Then the resist on the substrate was flushed with isopropanol and left to dry before the inspection. The silicon wafer was cleaved into several rectangular slides, each containing 625 microcontainers. The height and inner diameter of the resulting microcontainers were 220 and 190 μm, respectively, with a 25 μm-thick sealed bottom. A diced chip was torn off and placed in a sample holder. A very thin layer of PDMS mixture acting as a negative mask (PDMS monomers mixed with Iguracure D2959 at the volume ratio of 10:1) was spread across the spaces between the microwells. Then, PDMS was fully cured in an oven at 37 °C overnight.

Loading of TRAP Microdevices. Ascorbic acid, $FeCl_3$ (III), and PEGDA monomer (Mn: 575) were purchased from Sigma-Aldrich, Denmark and were used with no pretreatment. Ascorbic acid and $FeCl_3$ (III), serving as redox initiators, were mixed uniformly at a weight ratio of 5:1 (w/w) with a mortar and pestle and stored in a vacuum chamber at room temperature. A modified brush loading method was used to load the resulting reactant mixture into the TRAP bots (with PDMS negative mask). Then a thin layer of PEGDA monomer (~20 μL) was evenly spread over the microcontainers using a doctor blading technique. The resulting TRAP bots were dried and kept in a dry environment. Lastly, the negative PDMS mask was peeled off, followed by the characterization and *in vitro* and *in vivo* studies.

Rhodamine 6G dye (R6G) (Sigma-Aldrich, Danmark) was used without any pretreatment to stain the PEGDA hydrogel for easy visualization (it is not part of the standard reaction mixture). R6G was distributed in radical initiators at a weight ratio of 1:50 (w/w) using a mortar and pestle. The resulting mixtures were loaded in TRAP bots and covered with a layer of PEGDA monomer as described in the above method. The assembled bots were dried at 40 °C for 24 h on a hot plate. A Carl Zeiss optical microscope Scope A1 coupled with bright-field, dark-field, and C-DIC mode was used to visualize TRAP bots activation. Video S1 shows homogeneous activation of multiple TRAP microdevices with R6G as a visual indicator (25 fps; speed 2×)

Fluorescein isothiocyanate (FITC)-insulin was mixed with reactant agents at a weight ratio of 1:50 and loaded into microcontainers to fabricate the TRAP bots using the same method as was used to prepare R6G-containing TRAP bots. The chip with FITC-insulin TRAP bots was placed in a plastic dish and wrapped with tinfoil. Twenty min of UV irradiation was used to sterilize the TRAP bots prior to cell studies.

***In Vitro* TRAP Bots Cell Study.** *Cell Culture.* Caco-2 and HT29-MTX-E12 cells were cultured in 75 mm^2 tissue culture flasks in Dulbecco's modified Eagle medium containing 4.5 g/L glucose (Sigma, Denmark) supplemented with 10% (v/v) heat-inactivated fetal bovine serum (Sigma, Denmark), 1% (v/v) non-essential amino acids (Gibco, Denmark), and 1% (v/v) penicillin-streptomycin (Gibco, Denmark). Cells were maintained at 37 °C and 5% CO_2 levels in a humidifying incubator. Cells were subcultured once they reached 70−80% confluence using a trypsin/ETDA solution (0.05%; Sigma, Denmark). All cells used for experiments were between passages 8 and 40.

Cell Trapping Studies. Cell trapping study was performed on a co-culture after 7 days. The media was removed from the wells, and seven TRAP bots were placed on top of the cell layer. 200 μL of fresh medium was added to each well and incubated for 4 h.

***In Vivo* Rat Study.** TRAP microdevices were loaded into a Torpac size 9 gelatin capsule which was coated in a 12% (w/v) Eudragit L100 solution in IPA with dibutyl sebacate as plasticizer in a 5% w/w ratio relative to Eudragit. Each size 9 capsule has *ca.* 600 microdevices.

Male Sprague−Dawley rats (Janvier Laboratories, Le Genest-Saint-Isle, France) were housed in groups of six per cage and allowed to acclimatize for at least 1 week with a reversed 12/12 h day/night cycle. Fasting of the rats was initiated 12−16 h prior to the studies, and the study was conducted under full anesthesia. The abdominal cavity was opened after which an enteric-coated capsule with a tiny permanent magnet (size: 0.2 cm × 0.1 cm; 1.3 T) inside was administered to the stomach using a gavage dosing tube. The capsule was dragged to the duodenum using an external NdFeB magnet (1.3 T). It must be noted that the role of magnet was only to drag the enteric-coated capsule across the stomach into the duodenum, after which, the capsule disintegrated and microdevices were released in the

https://dx.doi.org/10.1021/acsnano.0c05426
ACS Nano 2020, 14, 12072−12081

small intestine. A more detailed protocol is included in the Supporting Information.

GI Tract Protein Biomarker Quantification. Isolated TRAP microdevices were used for quantification of proteolytic enzyme (trypsin) as a model biomarker. Trypsin cleaves a succinylated casein substrate to generate peptide fragments with free amino-terminal groups. These peptides reacted with 2,4,6-trinitrobenzenesulfonic acid (TNBSA), followed by the measurement of the absorbance increase that results from the formation of yellow colored TNB-peptide adducts (λ_{max} = 405 nm). Please refer to supplementary section for a more detailed protocol.

Sample Preparation for Amplicon Sequencing. All microdevices were excised from the gut tissue of the rat model. Sample 1 (scrapped mucus with TRAPs): Mucus layer from the excised tissue was gently scrapped off with a stainless steel spatula together with TRAP microdevices. This sample was kept in an Eppendorf tube and stored at −20 °C until further use. Sample 2 (multiwash-TRAPs): TRAP bots were taken from the ileum tissue and washed three times, each with acetate buffer (pH 4), PBS, 70% EtOH, 2 min each with vigorous vortex, that is, a total of nine washes for each microdevice. Sample 3 (PBS-wash TRAPs) was prepared the same way as above but only utilized PBS for washing (three times), 2 min each cycle with vigorous vortex. The DNA extraction from the TRAP microdevices was performed by using the PureLink Microbiome DNA Purification Kit. The sequencing library was prepared using the standard Illumina MiSeq protocol for amplicon sequencing, using the V3−V4 primer regions, and analyzed *via* a BION pipeline. A more detailed protocol with secondary index PCR measurement is given in the Supporting Information.

ASSOCIATED CONTENT

Supporting Information

The Supporting Information is available free of charge at https://pubs.acs.org/doi/10.1021/acsnano.0c05426.

Video S1: Real-time hydrogel formation in multiple TRAP microdevices (MP4)

Figure S1: SEM micrographs of activated TRAP microdevice. Figure S2: Confocal fluorescence microscopy image of enmeshed bacteria-hydrogel. Figure S3: Optical microscopy images and SEM micrographs of TRAP microdevices after animal experiment. Figure S4: Protein (trypsin) biomarker assessment. Figure S5: Rarefaction curves for samples 1−4. Figure S6: Heatmap of the 25 most abundant genera arranged with respect to sample 1 (gut tissue only). Table S1: Secondary index PCR data of samples 1−4 (PDF)

AUTHOR INFORMATION

Corresponding Author

Sarvesh Kumar Srivastava − *The Danish National Research Foundation and Villum Foundation's Center for Intelligent Drug Delivery and Sensing Using Microcontainers and Nanomechanics (IDUN), Department of Health Technology, Technical University of Denmark, 2800 Kongens Lyngby, Denmark;* orcid.org/0000-0002-9723-0632; Email: sksr@dtu.dk

Authors

Lu Chen − *The Danish National Research Foundation and Villum Foundation's Center for Intelligent Drug Delivery and Sensing Using Microcontainers and Nanomechanics (IDUN), Department of Health Technology, Technical University of Denmark, 2800 Kongens Lyngby, Denmark*

Lina Gruzinskyte − *The Danish National Research Foundation and Villum Foundation's Center for Intelligent Drug Delivery and Sensing Using Microcontainers and Nanomechanics (IDUN), Department of Health Technology, Technical University of Denmark, 2800 Kongens Lyngby, Denmark; Department of Pharmacy, Faculty of Health and Medical Sciences, University of Copenhagen, 2100 København Ø, Denmark*

Steffen Lynge Jørgensen − *Danish Meat Research Institute, Danish Technological Institute, 2630 Taastrup, Denmark*

Anja Boisen − *The Danish National Research Foundation and Villum Foundation's Center for Intelligent Drug Delivery and Sensing Using Microcontainers and Nanomechanics (IDUN), Department of Health Technology, Technical University of Denmark, 2800 Kongens Lyngby, Denmark*

Complete contact information is available at: https://pubs.acs.org/10.1021/acsnano.0c05426

Author Contributions

S.K.S. conceived the idea, performed preliminary experiments, and invented the concept of self-polymerizing system for sampling of intestinal lumen. S.K.S. and L.C. fabricated TRAP microdevices. L.C. performed release studies. L.C. and L.G. performed cell studies and confocal fluorescence microscopy studies. S.L.J. performed 16s amplicon sequencing and processing of sequencing data. S.K.S. performed optical and SEM imaging, FT-IR spectroscopy, and discussion of sequencing data. L.C., L.G., and S.K.S. co-wrote the manuscript and prepared figures for the manuscript. A.B. provided infrastructural support, identified the possibility of applying microdevices in microbiota sampling, and revised the manuscript. All authors discussed the results and commented on the manuscript.

Notes

The authors declare no competing financial interest.

ACKNOWLEDGMENTS

All authors acknowledge the assistance of Lasse Højlund Eklund Thamdrup (DTU Healthtech) for microfabrication, Jacob Rune Jørgensen (University of Copenhagen) for *in vivo* experiments, and Tim Kåre Jensen (Center for Diagnostik, DTU) for Histology. S.K.S. would like to thank H. C. Ørsted COFUND for funding. This project has received funding from the European Union's Horizon 2020 research and innovation program under the Marie Skłodowska-Curie grant agreement no. 713683. All authors would like to acknowledge the Danish National Research Foundation (DNRF122) and Villum Fonden (grant no. 9301) for Intelligent Drug Delivery and Sensing Using Microcontainers and Nanomechanics (IDUN).

REFERENCES

(1) Huttenhower, C.; Gevers, D.; Knight, R.; Abubucker, S.; Badger, J. H.; Chinwalla, A. T.; Creasy, H. H.; Earl, A. M.; Fitzgerald, M. G.; Fulton, R. S.; Giglio, M. G.; Hallsworth-Pepin, K.; Lobos, E. A.; Madupu, R.; Magrini, V.; Martin, J. C.; Mitreva, M.; Muzny, D. M.; Sodergren, E. J.; Versalovic, J.; et al. Structure, Function and Diversity of the Healthy Human Microbiome. *Nature* **2012**, *486*, 207−214.

(2) Eckburg, P. B.; Bik, E. M.; Bernstein, C. N.; Purdom, E.; Dethlefsen, L.; Sargent, M.; Gill, S. R.; Nelson, K. E.; Relman, D. A. Microbiology: Diversity of the Human Intestinal Microbial Flora. *Science* **2005**, *308*, 1635−1638.

(3) Hillman, E. T.; Lu, H.; Yao, T.; Nakatsu, C. H. Microbial Ecology along the Gastrointestinal Tract. *Microbes and Environments* **2017**, *32*, 300−313.

(4) Matsumoto, H.; Kuroki, Y.; Higashi, S.; Goda, K.; Fukushima, S.; Katsumoto, R.; Oosawa, M.; Murao, T.; Ishii, M.; Oka, K.; Takahashi, M.; Osaki, T.; Kamiya, S.; Shiotani, A. Analysis of the Colonic Mucosa Associated Microbiota (MAM) Using Brushing Samples during Colonic Endoscopic Procedures. *J. Clin. Biochem. Nutr.* **2019**, *65*, 132−137.
(5) Biehl, L. M.; Garzetti, D.; Farowski, F.; Ring, D.; Koeppel, M. B.; Rohde, H.; Schafhausen, P.; Stecher, B.; Vehreschild, M. J. G. T. Usability of Rectal Swabs for Microbiome Sampling in a Cohort Study of Hematological and Oncological Patients. *PLoS One* **2019**, *14*, e0215428.
(6) Allaband, C.; McDonald, D.; Vázquez-Baeza, Y.; Minich, J. J.; Tripathi, A.; Brenner, D. A.; Loomba, R.; Smarr, L.; Sandborn, W. J.; Schnabl, B.; Dorrestein, P.; Zarrinpar, A.; Knight, R. Microbiome 101: Studying, Analyzing, and Interpreting Gut Microbiome Data for Clinicians. *Clin. Gastroenterol. Hepatol.* **2019**, *17*, 218−230.
(7) Breger, J. C.; Yoon, C.; Xiao, R.; Kwag, H. R.; Wang, M. O.; Fisher, J. P.; Nguyen, T. D.; Gracias, D. H. Self-Folding Thermo-Magnetically Responsive Soft Microgrippers. *ACS Appl. Mater. Interfaces* **2015**, *7*, 3398−3405.
(8) Srivastava, S. K.; Ajalloueian, F.; Boisen, A. Thread-Like Radical-Polymerization *via* Autonomously Propelled (TRAP) Bots. *Adv. Mater.* **2019**, *31*, 1901573.
(9) Wei, X.; Beltrán-Gastélum, M.; Karshalev, E.; Esteban-Fernández De Ávila, B.; Zhou, J.; Ran, D.; Angsantikul, P.; Fang, R. H.; Wang, J.; Zhang, L. Biomimetic Micromotor Enables Active Delivery of Antigens for Oral Vaccination. *Nano Lett.* **2019**, *19*, 1914−1921.
(10) De Ávila, B. E. F.; Angsantikul, P.; Li, J.; Angel Lopez-Ramirez, M.; Ramírez-Herrera, D. E.; Thamphiwatana, S.; Chen, C.; Delezuk, J.; Samakapiruk, R.; Ramez, V.; Obonyo, M.; Zhang, L.; Wang, J. Micromotor-Enabled Active Drug Delivery for *In Vivo* Treatment of Stomach Infection. *Nat. Commun.* **2017**, *8*, 272.
(11) Srivastava, S. K.; Clergeaud, G.; Andresen, T. L.; Boisen, A. Micromotors for Drug Delivery *In Vivo*: The Road Ahead. *Adv. Drug Delivery Rev.* **2019**, *138*, 41−55.
(12) Mandsberg, N. K.; Christfort, J. F.; Kamguyan, K.; Boisen, A.; Srivastava, S. K. Orally Ingestible Medical Devices for Gut Engineering. *Adv. Drug Delivery Rev.* **2020**, DOI: 10.1016/j.addr.2020.05.004.
(13) Malinowska, K. H.; Verdorfer, T.; Meinhold, A.; Milles, L. F.; Funk, V.; Gaub, H. E.; Nash, M. A. Redox-Initiated Hydrogel System for Detection and Real-Time Imaging of Cellulolytic Enzyme Activity. *ChemSusChem* **2014**, *7*, 2825−2831.
(14) Srivastava, S. K.; Ajalloueian, F.; Boisen, A. TRAP Technology: Thread-Like Radical-Polymerization *via* Autonomously Propelled (TRAP) Bots. *Adv. Mater.* **2019**, *31*, 1970213.
(15) Sarac, A. S. Redox Polymerization. Progress in Polymer Science. *Prog. Polym. Sci.* **1999**, *24*, 1149−1204.
(16) Walling, C.; Goosen, A. Mechanism of the Ferric Ion Catalyzed Decomposition of Hydrogen Peroxide. Effect of Organic Substrates. *J. Am. Chem. Soc.* **1973**, *95*, 2987−2991.
(17) Gallard, H.; De Laat, J.; Legube, B. Spectrophotometric Study of the Formation of Iron(III)-Hydroperoxy Complexes in Homogeneous Aqueous Solutions. *Water Res.* **1999**, *33*, 2929−2936.
(18) Xue, X.; Hanna, K.; Deng, N. Fenton-Like Oxidation of Rhodamine B in the Presence of Two Types of Iron (II, III) Oxide. *J. Hazard. Mater.* **2009**, *166*, 407−414.
(19) Perez-Benito, J. F. Iron(III)-Hydrogen Peroxide Reaction: Kinetic Evidence of a Hydroxyl-Mediated Chain Mechanism. *J. Phys. Chem. A* **2004**, *108*, 4853−4858.
(20) Barb, W. G.; Baxendale, J. H.; George, P.; Hargrave, K. R. Reactions of Ferrous and Ferric Ions with Hydrogen Peroxide. Part II. - The Ferric Ion Reaction. *Trans. Faraday Soc.* **1951**, *47*, 462−500.
(21) Teodorescu, M.; Gaynor, S. G.; Matyjaszewski, K. Halide Anions as Ligands in Iron-Mediated Atom Transfer Radical Polymerization. *Macromolecules* **2000**, *33*, 2335−2339.
(22) Perrier, S. 50th Anniversary Perspective: RAFT Polymerization - A User Guide. *Macromolecules* **2017**, *50*, 7433−7447.
(23) Haward, S. J.; Hopkins, C. C.; Shen, A. Q. Asymmetric Flow of Polymer Solutions around Microfluidic Cylinders: Interaction between Shear-Thinning and Viscoelasticity. *J. Non-Newtonian Fluid Mech.* **2020**, *278*, 104250.
(24) Fang, H.; Jiang, F.; Wu, Q.; Ding, Y.; Wang, Z. Supertough Polylactide Materials Prepared through *In Situ* Reactive Blending with PEG-Based Diacrylate Monomer. *ACS Appl. Mater. Interfaces* **2014**, *6*, 13552−13563.
(25) Narayan, S.; Rajagopalan, A.; Reddy, J. S.; Chadha, A. BSA Binding to Silica Capped Gold Nanostructures: Effect of Surface Cap and Conjugation Design on Nanostructure-BSA Interface. *RSC Adv.* **2014**, *4*, 1412−1420.
(26) Ponnuvelu, D. V.; Kim, S.; Lee, J. Polyethyleneglycol Diacrylate Hydrogels with Plasmonic Gold Nanospheres Incorporated *via* Functional Group Optimization. *Micro Nano Syst. Lett.* **2017**, *5*, 21−29.
(27) Varum, F. J. O.; Veiga, F.; Sousa, J. S.; Basit, A. W. Mucus Thickness in the Gastrointestinal Tract of Laboratory Animals. *J. Pharm. Pharmacol.* **2012**, *64*, 218−227.
(28) Johansson, M. E. V.; Gustafsson, J. K.; Holmen-Larsson, J.; Jabbar, K. S.; Xia, L.; Xu, H.; Ghishan, F. K.; Carvalho, F. A.; Gewirtz, A. T.; Sjovall, H.; Hansson, G. C. Bacteria Penetrate the Normally Impenetrable Inner Colon Mucus Layer in Both Murine Colitis Models and Patients with Ulcerative Colitis. *Gut* **2014**, *63*, 281−291.
(29) Lai, S. K.; Wang, Y. Y.; Wirtz, D.; Hanes, J. Micro- and Macrorheology of Mucus. *Adv. Drug Delivery Rev.* **2009**, *61*, 86−100.
(30) Curt, J. R.; Pringle, R. Viscosity of Gastric Mucus in Duodenal Ulceration. *Gut* **1969**, *10*, 931−934.
(31) Yildiz, H. M.; McKelvey, C. A.; Marsac, P. J.; Carrier, R. L. Size Selectivity of Intestinal Mucus to Diffusing Particulates Is Dependent on Surface Chemistry and Exposure to Lipids. *J. Drug Target.* **2015**, *23*, 768−774.
(32) Autian, J. Structure-Toxicity Relationships of Acrylic Monomers. *Environ. Health Perspect.* **1975**, *11*, 141−152.
(33) Williams, G. M.; Iatropoulos, M. J. Evaluation of Potential Human Carcinogenicity of the Synthetic Monomer Ethyl Acrylate. *Regul. Toxicol. Pharmacol.* **2009**, *53*, 6−15.
(34) Li, D.; Chen, H.; Mao, B.; Yang, Q.; Zhao, J.; Gu, Z.; Zhang, H.; Chen, Y. Q.; Chen, W. Microbial Biogeography and Core Microbiota of the Rat Digestive Tract. *Sci. Rep.* **2017**, *7*, 45840.
(35) Ketabi, A.; Dieleman, L. A.; Gänzle, M. G. Influence of Isomalto-Oligosaccharides on Intestinal Microbiota in Rats. *J. Appl. Microbiol.* **2011**, *110*, 1297−1306.
(36) Molin, G.; Johansson, M. L.; Ståhl, M.; Ahrné, S.; Andersson, R.; Jeppsson, B.; Bengmark, S. Systematics of the Lactobacillus Population on Rat Intestinal Mucosa with Special Reference to Lactobacillus Reuteri. *Antonie van Leeuwenhoek* **1992**, *61*, 175−183.
(37) Gerritsen, J.; Timmerman, H. M.; Fuentes, S.; van Minnen, L. P.; Panneman, H.; Konstantinov, S. R.; Rombouts, F. M.; Gooszen, H. G.; Akkermans, L. M. A.; Smidt, H.; Rijkers, G. T. Correlation between Protection against Sepsis by Probiotic Therapy and Stimulation of a Novel Bacterial Phylotype. *Appl. Environ. Microbiol.* **2011**, *77*, 7749−7756.
(38) Gerritsen, J.; Fuentes, S.; Grievink, W.; van Niftrik, L.; Tindall, B. J.; Timmerman, H. M.; Rijkers, G. T.; Smidt, H. Characterization of Romboutsia Ilealis Gen. Nov., Sp. Nov., Isolated from the Gastro-Intestinal Tract of a Rat, and Proposal for the Reclassification of Five Closely Related Members of the Genus Clostridium into the Genera Romboutsia Gen. Nov. *Int. J. Syst. Evol. Microbiol.* **2014**, *64*, 1600−1616.
(39) Sartor, R. B. Gut Microbiota: Optimal Sampling of the Intestinal Microbiota for Research. *Nat. Rev. Gastroenterol. Hepatol.* **2015**, *12*, 253−257.